

Cite this: *Chem. Sci.*, 2023, 14, 10768

All publication charges for this article have been paid for by the Royal Society of Chemistry

# Structurally divergent enantioselective synthesis of benzofuran fused azocine derivatives and spiro-cyclopentanone benzofurans enabled by sequential catalysis†

Rupkumar Khuntia,<sup>a</sup> Sanat Kumar Mahapatra,<sup>b</sup> Lisa Roy<sup>b</sup> and Subhas Chandra Pan<sup>b</sup>

An important objective in organic synthesis and medicinal chemistry is the capacity to access structurally varied and complex molecules rapidly and affordably from easily available starting materials. Herein, a protocol for the structurally divergent synthesis of benzofuran fused azocine derivatives and spiro-cyclopentanone benzofurans has been developed *via* chiral bifunctional urea catalyzed reaction between aurone-derived  $\alpha,\beta$ -unsaturated imine and ynone followed by switchable divergent annulation reactions by Lewis base catalysts (DBU and PPh<sub>3</sub>) with concomitant epimerization. The skeletally diversified products were formed in high yields with high diastereo- and enantioselectivities. Computational analysis with DFT and accurate DLPNO-CCSD(T) has been employed to gain deeper insights into mechanistic intricacies and investigate the role of chiral and Lewis base catalysts in skeletal diversity.

Received 26th June 2023  
Accepted 4th September 2023

DOI: 10.1039/d3sc03239f

rsc.li/chemical-science

## Introduction

In recent years, significant attention has been given to the development of concise, green and efficient methodologies for the preparation of target molecules.<sup>1</sup> Divergent synthesis is a fascinating and efficient strategy that has attracted much attention from chemists for the synthesis of diverse isomers with different chemo-, regio- or diastereoselectivities from identical starting materials.<sup>2–4</sup> In fact, synthesis of two or more structurally and stereogenically different types of chiral products *via* a divergent strategy is quite attractive.<sup>2c</sup> The principal strategy that has been used for the development of enantioselective divergent reactions is to employ different chiral catalysts to obtain product selectivity *via* different catalytic intermediates (catalyst controlled selectivity) (Scheme 1a).<sup>3d–s</sup> On the other hand, it is quite challenging to obtain structurally different compounds using the same chiral catalyst and with different additives or reagents or varying reaction conditions (additive or reagent controlled).<sup>3a–c,t–x</sup> In an early study, Jørgensen and co-workers reported an additive-controlled divergent synthesis of tetrahydrothiophenes using a diaryl prolinol TMS ether catalyst

(Scheme 1b).<sup>3a</sup> Interestingly, the authors observed different product formations using different additives, *i.e.*, PhCOOH and NaHCO<sub>3</sub>. Recently, the groups of Wang and Xu reported solvent dependent organocatalytic divergent reactions.<sup>3u,v</sup> In the current work, we describe a unique divergent process by sequential catalysis<sup>4</sup> where the first step uses a bifunctional catalyst and in the second step, the chiral intermediate participates in Lewis base controlled divergent annulation reactions (Scheme 1c). This method presents organocatalytic cycle-varying cascade reactions utilizing aurone-derived  $\alpha,\beta$ -unsaturated imine.

Previously the groups of Huang, Cheng and Zhai reported achiral divergent reactions with aurone-derived  $\alpha,\beta$ -unsaturated imine.<sup>5</sup> To the best of our knowledge, the catalytic asymmetric divergent reaction is still not known using an aurone-derived  $\alpha,\beta$ -unsaturated imine. Also, benzofuran or indole-fused eight-membered rings containing a nitrogen atom (azocines) are important structural motifs that are prevalent in many natural products and biologically active molecules such as PKD inhibitor kb-NB96-53, balasubramide, grandilodine A, *etc.*<sup>6</sup> The efficient construction of eight-membered rings in such molecular structures is a fundamental synthetic challenge.<sup>7</sup> The inherent strains of the targeted azocines, as well as competing pathways leading to either the highly favoured six- or five-membered rings are the key hindrances for the formation of eight-membered rings. We envisioned that a benzofuran/indole-derived nitrogen-containing electrophilic partner such as aurone-derived  $\alpha,\beta$ -unsaturated imine<sup>8</sup> could be coupled with alkynyl ketones<sup>9</sup> to deliver azocine. Similarly, spiro-cyclopentane benzofuran motifs are present in many bioactive natural

<sup>a</sup>Department of Chemistry, Indian Institute of Technology Guwahati, Assam, 781039, India. E-mail: span@iitg.ac.in; Web: <https://www.iitg.ac.in/span/>

<sup>b</sup>Institute of Chemical Technology Mumbai IOC Odisha Campus Bhubaneswar, Bhubaneswar 751013, India

† Electronic supplementary information (ESI) available: Experimental details, characterization and analytical data. CCDC 2235079(3f) and 2235267(4k). For ESI and crystallographic data in CIF or other electronic format see DOI: <https://doi.org/10.1039/d3sc03239f>





Scheme 1 Catalytic asymmetric divergent reactions.

products such as laurenistich-4-ol, spiroapplanatumine K and involucratustone B.<sup>10</sup> However, only a few catalytic asymmetric syntheses of spiro-cyclopentanone benzofurans are known.<sup>11</sup> Thus, an efficient route for the preparation of such a motif in enantioselective fashion is highly desirable. We speculated that such a motif can be generated by reacting only the C=C of aurone-derived  $\alpha,\beta$ -unsaturated imine. Herein, we would like to disclose our extensive explorations on these issues.

## Results and discussion

The initial experiment involved performing the reaction between *N*-sulfonyl 1-azadiene **1a** and ynone **2a** with bifunctional urea catalyst **I** in toluene at room temperature (Table 1, entry 1). A smooth conversion was observed in 12 hours to provide intermediate **A** with 1.7 : 1 dr, which after short column chromatography was treated with DBU. This resulted in an annulation reaction with concomitant epimerization<sup>12</sup> for the formation of thermodynamically stable *trans* benzofuran fused azocine derivative **3a** with 88% yield, >20 : 1 dr and 84% ee. Interestingly, Takemoto catalyst **II** with a thiourea motif afforded **3a** with much less enantioselectivity (Table 1, entry 2). A good enantioselectivity of 80% was detected with *t*-leucine derived bifunctional urea catalyst **III** but thiourea derivative **IV** was not effective (Table 1, entries 3–4). Then we screened *t*-leucine derived bifunctional squaramide catalyst **V** in the reaction and moderate enantioselectivity was obtained (Table 1,

Table 1 Catalyst and solvent optimization for azocine

Entry <sup>a</sup>	Catalyst	Solvent	Yield <sup>b</sup>	d.r. <sup>c</sup>	ee <sup>d</sup>
1	<b>I</b>	Toluene	88	>20 : 1	84
2	<b>II</b>	Toluene	57	>20 : 1	33
3	<b>III</b>	Toluene	89	>20 : 1	80
4	<b>IV</b>	Toluene	90	>20 : 1	5
5	<b>V</b>	Toluene	90	>20 : 1	67
6	<b>VI</b>	Toluene	90	>20 : 1	88
7	<b>VII</b>	Toluene	30	>20 : 1	12
8	<b>VIII</b>	Toluene	92	>20 : 1	77
9	<b>IX</b>	Toluene	55	>20 : 1	47
10	<b>X</b>	Toluene	<5	n.d	n.d
11	<b>VI</b>	Mesitylene	91	>20 : 1	82
12	<b>VI</b>	<i>o</i> -Xylene	77	>20 : 1	82
13 <sup>e</sup>	<b>VI</b>	Toluene	88	>20 : 1	88
14 <sup>f</sup>	<b>VI</b>	Toluene	91	>20 : 1	92

<sup>a</sup> Unless otherwise mentioned, reactions were carried out with 0.1 mmol of **1a** and 0.11 mmol of **2a** in 1 ml solvent at rt. <sup>b</sup> Isolated yield after silica gel column chromatography. <sup>c</sup> Determined by <sup>1</sup>H NMR. <sup>d</sup> Determined by chiral HPLC. <sup>e</sup> Reaction was run at 0 °C. <sup>f</sup> Reaction was run at –10 °C and for **2d**.

entry 5). Then we turned our attention to employ cinchona alkaloid derived bifunctional urea and thiourea catalysts and this proved to be effective.<sup>13</sup> Cinchonidine derived bifunctional urea catalyst **VI** promoted the reaction with 90% yield and 88% ee was observed (Table 1, entry 6). Thiourea derivative **VII** was not effective (Table 1, entry 7). Similar trends of enantioselectivities were observed with quinine derived bifunctional urea and thiourea catalysts **VIII** and **IX** (Table 1, entries 8–9). Bifunctional squaramide catalyst **X** also was not suitable for the reaction (Table 1, entry 10). Then we focused on the solvent optimization with catalyst **VI** (Table 1, entries 11–12). Slightly lower enantioselectivities were found in mesitylene and *o*-xylene solvents. Other solvents also could not improve the enantioselectivity (see the ESI† for details). Then the reaction was run in toluene at lower temperatures (Table 1, entries 13–14). Though the enantioselectivity did not change at 0 °C, the enantioselectivity improved to 92% ee after running the reaction at –10 °C for 2 days. Under these conditions, the enantioselectivities of the major and minor diastereomers of intermediate **A** were found to be 92% and 88% ees, respectively. A one-pot reaction



was also performed but the product **3a** was obtained in lower enantioselectivity (90% yield and 83% ee).

After finalizing the optimal reaction conditions, we set out to determine the substrate range for this new [4 + 4] annulation. Initially, the scope of azadiene **1** was checked and gratifyingly good results were obtained. As shown in Scheme 2, high to excellent enantioselectivities and good to high yields were obtained for a variety of azadienes with substitutions in the *ortho*, *meta*, and *para* positions of the phenyl group. 4-Methyl and 4-methoxy substituted azadienes **1b** and **1d** provided products **3b** and **3d** in 87% and 89% ees, respectively. Slightly lower enantioselectivity was detected for product **3c** having 4-*t*-butyl substitution. Halo substitutions were also tolerated and high enantioselectivities were observed for products **3e** and **3f** having 4-fluoro and 4-bromo substitutions, respectively. A smooth conversion was also detected for compound **2g** having 4-CF<sub>3</sub> substitution and the desired product **3g** was isolated in 92% yield with 89% ee. The reaction outcome did not change with meta-substituted aryl group containing azadienes **1h** and **1i**, and high enantioselectivities were attained for products **3h** and **3i**. 2-Naphthyl containing azadiene **1j** also participated in the reaction to deliver product **3j** in 95% ee. Finally, 2-thienyl containing azadiene **1k** was engaged in the reaction and a good result was obtained for product **3k**. Then substitutions in the

benzofuran motif were examined, and pleasingly, methoxy- and bromo-substituted azadienes **1l** and **1m** reacted smoothly to provide products **3l** and **3m**, respectively, in 93% ee. Other groups, such as N-Ns and N-SO<sub>2</sub>Me groups, could be used in place of the N-Ts group; and high enantioselectivities were found for **3n** and **3o**. Then the scope of ynone **2** was examined and encouragingly positive outcomes were found (Scheme 2).

Initially the aryl group close to the carbonyl group was varied. Here also, different substitutions at the *ortho*-, *meta*- and *para*-positions were tolerated and excellent enantioselectivities were detected for the products **3p–3t**. High enantioselectivity was detected for compound **3u** having a 3,4-disubstituted aryl group. The reaction outcome did not change with 2-naphthyl substitution and product **3v** was isolated in 92% yield with 91% ee. Then the substitutions on the aryl group attached to the triple bond in **2** were checked. To our delight, good results were observed for products **3w–3y** having different *para*-substituted aryl groups. Slightly lower enantioselectivities were detected for products **3z** and **3z'** having *ortho*- and *meta*-substitutions, respectively.

Next, the chiral intermediate **A** (dr = 1.7 : 1) formed from the reaction of **1a** and **2a** was treated with 20 mol% triphenylphosphine in CH<sub>2</sub>Cl<sub>2</sub>. To our delight, after stirring for 12 hours, spiro-cyclopentanone benzofuran **4a** with a stereogenic quaternary centre was isolated in 90% yield with 7 : 1 dr and 92% ee (Scheme 3). Here also epimerization was observed. A one-pot reaction was also performed but spiro-benzofuran **4a** was isolated in 83% yield with 77% ee. The minor diastereomer originates from the creation of a stereogenic quaternary centre (see the ESI† for details). Then a variety of azadienes **1** were examined under sequential conditions, and encouragingly positive results were found. When several *para*-substitutions were first tested, the results for products **4b–4g** were pleasingly high in terms of diastereoselectivities and excellent in terms of enantioselectivities (Scheme 3). The outcome did not change with *meta*-substitutions and the products **4h** and **4i** were obtained in 92% and 91% ees, respectively. Naphthyl and thienyl substitutions were also tolerated and good results were detected for products **4j** and **4k**. Then, the benzofuran motif's substitutions were looked at, and it was pleasing to see that the methoxy- and bromo-substituted azadienes **1l** and **1m** reacted smoothly to produce products **4l** and **4m** in 93% ee (Scheme 3). Next, other imine protective groups were examined, and it was discovered that N-Ns and N-SO<sub>2</sub>Me groups containing azadienes produced positive results for the products **4n–4o**. Then the scope of ynone **2** was checked and here also excellent results were found with different aryl group variations incorporated at the  $\alpha$ -position of the carbonyl group of **2**. In fact, 89–92% ees were observed for products **4p–4v**. Then different substitutions on the aryl group attached to the triple bond in **2** were checked and excellent results were achieved for products **4w–4y** having different *para*-substitutions. The enantioselectivities slightly dropped with *ortho*- and *meta*-substitutions (both **4z** and **4z'** in 83% ee).

The absolute configuration of compound **3f** was determined to be (5*S*, 6*S*) by X-ray crystallography.<sup>14</sup> Thus other azocine derivatives **3** are expected to have the same configuration.



**Scheme 2** Scope of benzofuran fused azocines<sup>a,b</sup>. <sup>a</sup>All reactions were carried out with 0.1 mmol of **1** and 0.11 mmol of **2** in 1 ml toluene at  $-10$  °C for 2 days. Then, the isolated adduct was treated with DBU (20 mol%) in CH<sub>2</sub>Cl<sub>2</sub> (1 ml) at rt for 2 h. <sup>b</sup>Yields correspond to the isolated yields after silica gel column chromatography, dr was determined by <sup>1</sup>H NMR and in all cases >20 : 1; ee was determined by HPLC.

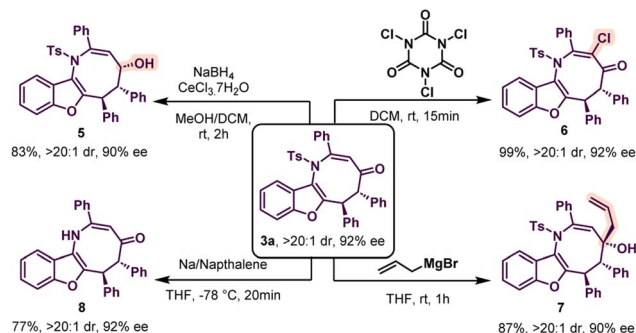




**Scheme 3** Scope of spiro-cyclopentanone benzofurans<sup>a,b</sup>. <sup>a</sup>All reactions were carried out with 0.1 mmol of **1** and 0.11 mmol of **2** in 1 ml toluene at  $-10\text{ }^{\circ}\text{C}$  for 2 days. Then, the isolated adduct was treated with  $\text{PPh}_3$  (20 mol%) in  $\text{CH}_2\text{Cl}_2$  (1 ml) at rt for 12 h. <sup>b</sup>Yields correspond to the isolated yields after silica gel column chromatography, dr was determined by  $^1\text{H}$  NMR, in all cases  $E/Z$  ratio  $>20:1$  and ee was determined by HPLC.

Similarly, the absolute configuration of **4k** was found to be ( $4'S$ ,  $5'S$ ) from X-ray crystallography.<sup>15</sup> Thus, other benzofurans **4** will have the same configuration. Then, azocine **3a** was subjected to a variety of organic transformations to further demonstrate the usefulness of our technique (Scheme 4). Initially, **3a** was treated with sodium borohydride and cerous chloride to provide **5** with an alcohol group in high diastereoselectivity and the enantioselectivity was almost retained. The relative configuration of **5** was determined by 2D NMR spectroscopy. Then a chlorination reaction was performed with trichloroisocyanuric acid (TCCA). This resulted in the formation of **6** in 99% yield and both diastereo- and enantioselectivity were unchanged. Then, allylation of **3a** was carried out with allyl magnesium bromide in THF. To our delight, the reaction proceeded smoothly to provide compound **7** as a single diastereomer with high enantioselectivity. Finally, deprotection of the *N*-tosyl group was performed and product **8** was formed without erosion in enantioselectivity.

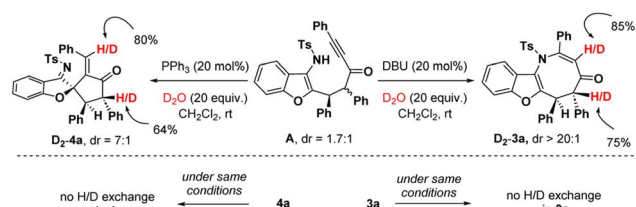
To get insight into the mechanism, we carried out deuteration experiments with intermediate **A** (Scheme 5). At first, **A** (1.7 : 1 dr) was treated with DBU (20 mol%) and  $\text{D}_2\text{O}$  (20 equiv.) in  $\text{CH}_2\text{Cl}_2$  at room temperature.  $^1\text{H}$  nuclear magnetic resonance (NMR) analysis of **3a** revealed 85% deuterium incorporation at



**Scheme 4** Synthetic transformations of azocine **3a**.

the C3-position and 75% deuterium incorporation at the C5-position. When **3a** was stirred under similar conditions, no H/D exchange was detected. Similarly, the deuteration reaction was performed with intermediate **A**,  $\text{PPh}_3$  (20 mol%) and  $\text{D}_2\text{O}$  (20 equiv.), and in fact, 80% deuterium incorporation was found at the olefin carbon and 64% deuterium incorporation was detected at the C4'-position of **4a**. No H/D exchange was noticed when **4a** was agitated in the same manner. This suggests that in both cases, the C2-center of **A** underwent an epimerization to deliver the stereoisomers in favour of the thermodynamically more stable *trans*-isomer.

Furthermore, computational studies with the density functional theory (DFT) at B3LYP-D3(BJ)/def2-TZVP/C-PCM//PBE-D3(BJ)/def2-SVP<sup>16</sup> were conducted in order to understand the origin of the enantioselectivity and divergence of the asymmetric product on switching of Lewis base catalysts. To ponder about the enantioselectivity of the azocine and spiro derivatives and probe the plausible catalytic activation modes, we chose the reaction between *N*-sulfonyl 1-azadiene, **1a**, and ynone, **2a**, in the presence of the cinchonidine derived bifunctional urea catalyst **VI** (Table 1, entry 6), and conducted an extensive computational study with both Re- and Si-face activation of the substrates (see the ESI†). The chiral reactant complex consisting of the substrates and the weakly bound catalyst in the Re-face ( $\text{RC}_{\text{re-ss}}$ ), resulting in the *S,S* configuration of the aurone-derived  $\alpha,\beta$ -unsaturated imine ( $\text{A}_{\text{re-ss}}$ , Fig. 1 inset), is significantly lower in energy as compared to the other adducts (see Fig. S2†). Indeed,  $\text{RC}_{\text{re-ss}}$  is highly exergonic ( $\Delta G = -10.4\text{ kcal mol}^{-1}$ ) as compared to the separated reactants and the catalyst. Hence it has been chosen as the reference for the Gibbs free energy profile as shown in Fig. 1. The nucleophilic attack of azadiene **1a** to the enol form of **2a** along the Re-face through the



**Scheme 5** Deuterium exchange experiment.



two transition states,  $\text{TS}_{\text{re-SS}}$  and  $\text{TS}_{\text{re-SR}}$ , resulting in major (*S,S*) and minor (*S,R*) enantiomers of the  $\alpha,\beta$ -unsaturated imine intermediate **A**, is predicted at a Gibbs free energy barrier of 11.5 and 13.5 kcal mol<sup>-1</sup> (Fig. 1), consistent with the experimental findings. Further refinement of energetics at the DLPNO-CCSD(T)/def2-TZVP/C-PCM//PBE-D3(BJ)/def2-SVP level of theory predicts the relative  $\Delta G^\ddagger$  at 9.2 and 13.3 kcal mol<sup>-1</sup>, respectively, which is in accordance with the stereochemical outcome. The lower activation energy requirement of  $\text{TS}_{\text{re-SS}}$  as compared to  $\text{TS}_{\text{re-SR}}$  is presumably due to extensive attractive non-covalent interactions such as  $\pi$ - $\pi$  and H-bond interactions (see Fig. S6<sup>†</sup>).<sup>17</sup> Furthermore, plots of the steric maps of  $\text{TS}_{\text{re-SS}}$  and  $\text{TS}_{\text{re-SR}}$  in Fig. 2 show that %  $V_{\text{free}}$ , which accounts for the percentage of total free volume within the catalyst pocket, has similar values.<sup>18</sup> However, a careful investigation reveals that %  $V_{\text{free}}$  in the south-east quadrant, where the C-C coupling between the two substrates takes place is significantly lower for  $\text{TS}_{\text{re-SR}}$  (21.8%) as compared to that for  $\text{TS}_{\text{re-SS}}$  (35.3%). A smaller value of %  $V_{\text{free}}$  indicates greater confinement and thereby more steric encumbrance. Hence the “open” structure within the catalytic pocket, with lowered steric congestion, along with the complimentary attractive non-covalent interactions results in  $\text{TS}_{\text{re-SS}}$ , predicted to be always more stabilized than  $\text{TS}_{\text{re-SR}}$  (see the ESI<sup>†</sup>).<sup>19</sup> Incidentally, in the absence of **VI**, the reaction between the enol form of **2a** and **1a** is estimated at high energetic expenses (see Fig. S1<sup>†</sup>), further emphasizing the crucial role of the H-bond networks offered by the chiral catalyst. The catalytic *Si*-face activation of the substrates is predicted at predominantly high barriers (see Fig. S2<sup>†</sup>) and rationalizes the significance of the *Re*-face approach for a favourable attack. Next, we explored the intramolecular cyclization of  $\alpha,\beta$ -unsaturated imine intermediate **A** in the presence of the Lewis base catalyst, DBU (Fig. 3). Starting from the reactant complex  $\text{RC}_{\text{D-SS}}$  consisting of the major enantiomer  $\text{A}_{\text{re-SS}}$  together with DBU, we envisage a 1,4-addition of DBU towards the electrophilic alkyne

carbon centre of  $\text{A}_{\text{re-SS}}$  via  $\text{TS1}_{\text{D-SS}}$  at an energetic expense of 12.4 kcal mol<sup>-1</sup>. Expectedly, a similar attack by DBU on  $\text{A}_{\text{re-SR}}$  via  $\text{TS1}_{\text{D-SR}}$  requires more than 7.0 kcal mol<sup>-1</sup> free energy of activation, primarily due to the absence of an intramolecular H-bond unlike  $\text{RC}_{\text{D-SS}}$  and  $\text{TS1}_{\text{D-SS}}$ , and the subsequent reaction, leading to the (*S,R*) product, **4<sub>SR</sub>** as shown in the ESI (see Fig. S3<sup>†</sup>). The resultant chiral  $\alpha,\beta$ -unsaturated zwitterion,  $\text{I}_{\text{D-SS}}$ , quickly reorganizes to the allene  $\text{II}_{\text{D-SS}}$  on N-H-shifting with a barrier-less rotation followed by an energetically favourable keto-enol tautomerism to the  $\alpha,\beta$ -unsaturated keto intermediate,  $\text{III}_{\text{D-SS}}$ , crucial for the emergence of the azocine and the spiro compounds. The trajectory for the formation of the eight membered cyclized azocine derivative **3a<sub>SS</sub>** proceeds through a stepwise intramolecular nucleophilic attack of the N-centre on the electrophilic  $\beta$ -sp<sup>2</sup>-C centre *via*  $\text{TS2}_{\text{D-SS}}$  and DBU release *via*  $\text{TS4}_{\text{D-SS}}$  (Fig. 3). In a similar way, the other diastereomer  $\text{RC}_{\text{D-SR}}$  reacts through  $\text{I}_{\text{D-SR}}$ ,  $\text{II}_{\text{D-SR}}$  and  $\text{III}_{\text{D-SR}}$  (see the ESI<sup>†</sup>) intermediates. The intermediate  $\text{III}_{\text{D-SR}}$  undergoes a rapid epimerization to generate the thermodynamically stable  $\text{III}_{\text{D-SS}}$  through intermediate **XD**, which facilitates generation of **3a** with high diastereoselectivity. Alternatively, a six membered cyclized plausible product, **3a'<sub>SS</sub>**, is hypothesized through a concerted transition state,  $\text{TS3}_{\text{D-SS}}$ . The chemoselectivity for the observed 8 membered azocine product over the six-membered analogue is evident from  $\Delta\Delta G = 1.4$  kcal mol<sup>-1</sup>. Indeed, the higher selectivity of the H-bond assisted C-N cyclization step over C-C cyclization is also supported at the DLPNO-CCSD(T)/def2-TZVP level of theory ( $\Delta\Delta G^\ddagger = 4.1$  kcal mol<sup>-1</sup>), nullifying the possibility of the C-C coupling analogue. In contrast,  $\text{A}_{\text{re-SS}}$  delivers a highly stable five membered spiro compound **4a<sub>SS</sub>** in the presence of  $\text{PPh}_3$  (Fig. 4).

The chiral reactant complexes,  $\text{RC}_{\text{P-SS}}$  and  $\text{RC}_{\text{P-SR}}$ , consisting of the two diastereomers,  $\text{A}_{\text{re-SS}}$  and  $\text{A}_{\text{re-SR}}$ , together with  $\text{PPh}_3$  are predicted to be equi-energetic (Fig. 4). Evidently, the higher stability of  $\text{TS1}_{\text{P-SS}}$  ( $\Delta G^\ddagger = 8.8$  kcal mol<sup>-1</sup>) than  $\text{TS1}_{\text{P-SR}}$  ( $\Delta G^\ddagger =$

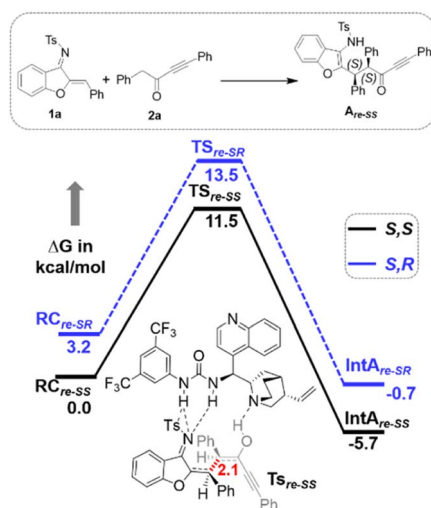


Fig. 1 Gibbs free energy (kcal mol<sup>-1</sup>) profile at B3LYP-D3(BJ)/CPCM(toluene)/def2-TZVP for bifunctional urea catalyst **VI** mediated **1a** and **2a** coupling. Distances shown are in units of Å.

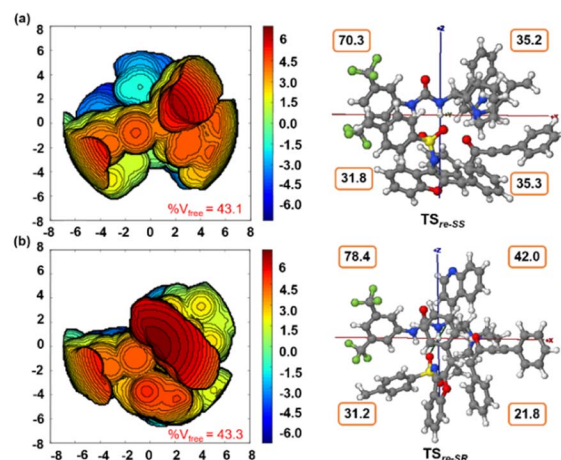


Fig. 2 Steric map (within a range of  $\pm 6.0$  kcal mol<sup>-1</sup>) and 3D model with xyz axes (between  $\pm 8$  Å) for (a)  $\text{TS}_{\text{re-SS}}$  and (b)  $\text{TS}_{\text{re-SR}}$ . Total %  $V_{\text{free}}$  and those in each quadrant along the xyz axes are shown. Contour color – blue: strong attractive; green: weak attractive; red: strong repulsive.



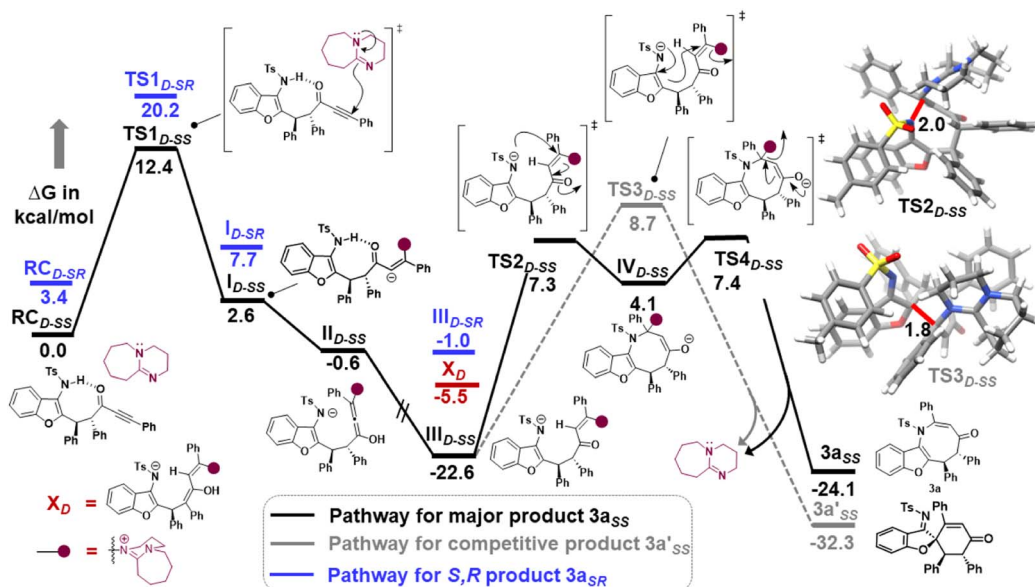


Fig. 3 Gibbs free energy ( $\text{kcal mol}^{-1}$ ) profile at B3LYP-D3(BJ)/CPCM( $\text{CH}_2\text{Cl}_2$ )/def2-TZVP for the DBU assisted intramolecular cyclization of intermediate  $A_{re-SS}$  and  $A_{re-SR}$ . Distances shown are in units of Å. Color code: C(grey), H(white), N(blue), O(red), and S(yellow). D sub-script denotes DBU assisted.

$15.3 \text{ kcal mol}^{-1}$ ), during nucleophilic attack of  $\text{PPh}_3$  on the  $\alpha$ ,  $\beta$ -unsaturated imine, drives the reaction towards the *S,S* enantiomer preferentially. This results in stable  $I_{P-SS}$  reorganizing to an allene rotamer  $II_{P-SS}$ , with a proton shift from the N-centre to the carbonyl O-atom along with the breakage of H-bonding. Subsequently, a free energetically and sterically stable keto-enol tautomer intermediate  $III_{P-SS}$  is formed which controls the

selectivity in the reaction. The delocalisation of the anionic electrons present over the N-atom to the C1 atom leads to the development of an intrinsic nucleophilic centre adjacent to furan O. This leads to an intramolecular nucleophilic umpolung attack on the  $\alpha$ - $\text{sp}^2$  C-centre at an energetic expense of  $13.1 \text{ kcal mol}^{-1}$  ( $TS2_{P-SS}$ ), to furnish a chiral spiro intermediate  $IV_{P-SS}$ . With a 1,2 H-shift, a stable  $V_{P-SS}$  is formed which

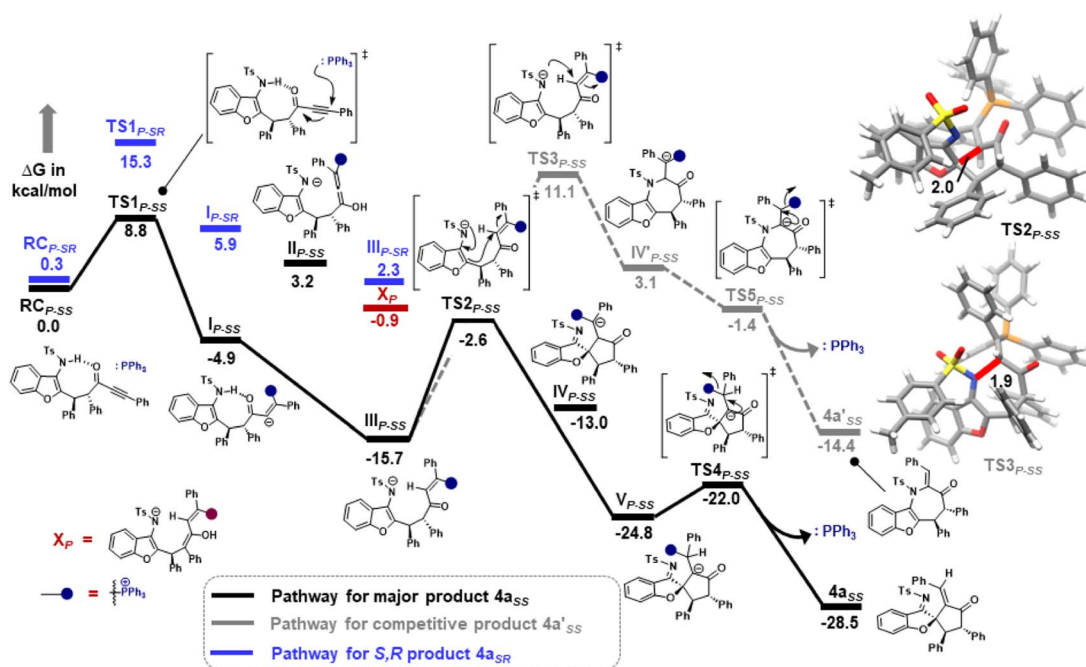


Fig. 4 Gibbs free energy ( $\text{kcal mol}^{-1}$ ) profile at B3LYP-D3(BJ)/CPCM( $\text{CH}_2\text{Cl}_2$ )/def2-TZVP for the  $\text{PPh}_3$  assisted intramolecular cyclization of intermediates  $A_{re-SS}$  and  $A_{re-SR}$ . Distances shown are in units of Å. Color code: C(grey), H(white), N(blue), O(red), and S(yellow). P subscript denotes  $\text{PPh}_3$  assisted.



subsequently releases  $\text{PPh}_3$  at an energy barrier of  $2.8 \text{ kcal mol}^{-1}$  ( $\text{TS4}_{\text{P-SS}}$ ) to generate the five membered chiral spiro compound,  $4\text{a}_{\text{SS}}$ . On the other hand, the minor diastereomer  $\text{RC}_{\text{P-SR}}$  delivers  $4\text{a}$  with high diastereoselectivity *via* epimerization through intermediate  $\text{X}_{\text{P}}$ . The study correlates an enol-tautomerization of  $\text{III}_{\text{P-SR}}$  to give energetically stable  $\text{X}_{\text{P}}$ , which subsequently epimerized to the thermally stable  $\text{III}_{\text{P-SS}}$  to produce the targeted product  $4\text{a}$ . The alternative pathway of intramolecular nucleophilic attack of N on the  $\alpha\text{-sp}^2$  C-centre through  $\text{TS3}_{\text{P-SS}}$  is ruled out due to the large energy drift. Hence, the formation of the seven membered  $4\text{a}'_{\text{SS}}$  is not feasible. This is supported by DLPNO-CCSD(T)/def2-TZVP energy barriers ( $\Delta\Delta G^\ddagger = 12.5 \text{ kcal mol}^{-1}$ ). Notably, DBU is found to be highly basic with a  $\text{p}K_{\text{a}}$  of 16.8 as compared to  $\text{PPh}_3$  having  $\text{p}K_{\text{a}} = 2.8$ .<sup>20</sup> One may fathom an alternative pathway consisting of a deprotonative activation of the  $\text{TsNH}$  moiety by Brønsted basic action of DBU, that leads to intramolecular cyclization through C–N attack. Indeed, formation of the eight-membered ring containing product,  $3\text{a}_{\text{SS}}$ , takes place at a barrier of  $19.4 \text{ kcal mol}^{-1}$ , while the six-membered ring containing C–C coupling TS leading to  $3\text{a}'_{\text{SS}}$  has to overcome a kinetic expense of  $23.5 \text{ kcal mol}^{-1}$ , further emphasizing the predominance of  $3\text{a}_{\text{SS}}$  as the product. To confirm the Brønsted or Lewis base pathway, we have recorded the ESI-MS spectrum of the reaction mixture, and a  $m/z$  of 748.3209 corresponding to  $[\text{M} + \text{H}^+]$  of intermediates  $\text{I}_{\text{D-SS}}$ ,  $\text{II}_{\text{D-SS}}$ , and  $\text{III}_{\text{D-SS}}$  was found. This ruled out the alternate path where DBU functions as a Brønsted base (see the ESI† for details).

As evident from our computational studies,<sup>21</sup> the cyclization processes in the presence of two different Lewis base catalysts turns out to be the rate determining steps (RDSs) and are responsible for the product selectivity, *i.e.*, predominance of  $3\text{a}_{\text{SS}}$  over  $3\text{a}'_{\text{SS}}$  and  $4\text{a}_{\text{SS}}$  over  $4\text{a}'_{\text{SS}}$ . A careful investigation shows that  $\text{TS2}_{\text{D-SS}}$  leading to the eight-membered cyclic core in  $3\text{a}_{\text{SS}}$  suffers from greater geometric distortion ( $\Delta\Delta E_{\text{dist}} = 13.9 \text{ kcal mol}^{-1}$ ) as compared to  $\text{TS3}_{\text{D-SS}}$  leading to the six-membered moiety in  $4'_{\text{SS}}$  (Fig. 5, see the ESI† for computational details). In contrast, the relative interaction energy ( $\Delta\Delta E_{\text{int}} = -16.0 \text{ kcal mol}^{-1}$ ) suggests a better orbital overlap and favourable electronic interactions for  $\text{TS2}_{\text{D-SS}}$  and stabilizes its energetic requirement by  $2.1 \text{ kcal mol}^{-1}$ . Interestingly, formation of the five-membered core in  $\text{TS2}_{\text{P-SS}}$  features greater  $\pi\text{-}\pi$  interactions coupled to lower steric encumbrance from the bulkier  $\text{PPh}_3$  additive that is reflected in their lower geometric distortion as compared to that of  $\text{TS3}_{\text{P-SS}}$  ( $\Delta\Delta E_{\text{dist}} = -33.6 \text{ kcal mol}^{-1}$ ). This easily overshoots the unfavourable interaction energy ( $\Delta\Delta E_{\text{int}} = 21.9 \text{ kcal mol}^{-1}$ ) and rationalises the observance of the 5-membered spiro compound,  $4\text{a}_{\text{SS}}$ .

In summary, we have developed a divergent pathway for the catalytic asymmetric synthesis of skeletally different benzofuran fused azocine derivatives and spiro-cyclopentanone benzofurans. The methodology involves sequential catalysis of a chiral bifunctional squaramide catalysed reaction between aurone-derived  $\alpha,\beta$ -unsaturated imine and ynone followed by Lewis base catalyzed divergent annulation reactions. In both cases, epimerization leads to high diastereoselectivity. Few synthetic transformations have also been performed.



Fig. 5 Energy decomposition analysis at B3LYP-D3(BJ)/CPCM( $\text{CH}_2\text{-Cl}_2$ )/def2-TZVP in units of  $\text{kcal mol}^{-1}$  for  $\text{TS2}_{\text{D-SS}}$ ,  $\text{TS3}_{\text{D-SS}}$ ,  $\text{TS2}_{\text{P-SS}}$  and  $\text{TS3}_{\text{P-SS}}$ .

Additionally, computational analysis has been performed to investigate the reaction mechanism and comprehend the chiral and Lewis base catalysts' control on the observed skeletal selectivity. Interestingly, London dispersive forces such as  $\pi\text{-}\pi$  and H-bond interactions are found to be crucial to overthrow the steric encumbrance for the stereochemical selectivity and achieve skeletal diversity. Given the significant medicinal value of azocines and spiro-cyclopentanone benzofurans, the pharmaceutical sector may find our procedure valuable.

## Data availability

All the experimental and computational data are available in ESI.†

## Author contributions

RK and SCP designed the experiment. RK performed the experiments. SKM and LR done the DFT study of the reactions.

## Conflicts of interest

There are no conflicts to declare.

## Acknowledgements

This work was supported by DST-SERB (file no CRG/2022/000698). We also thank CIF, Indian Institute of Technology Guwahati and North East Centre for Biological Sciences and Healthcare Engineering (NECBH), IIT Guwahati and Department of Biotechnology (DBT), Govt. of India (project no. BT/COE/34/SP28408/2018) for the instrumental facilities. We would also like to thank Abhay Pratap Singh of IIT Guwahati for his help in solving the X-ray structure. LR thanks SERB, India (SPG/2020/000754) for funding. SKM acknowledges the research fellowship of ICT-IOCB.



## Notes and references

- 1 (a) R. S. Doerksen, C. C. Meyer and M. J. Krische, *Angew. Chem., Int. Ed.*, 2019, **58**, 14055; (b) A. H. Hoveyda, Y. Zhou, Y. Shi, M. K. Brown, H. Wu and S. Torker, *Angew. Chem., Int. Ed.*, 2020, **59**, 21304; (c) S. Rej, Y. Ano and N. Chatani, *Chem. Rev.*, 2020, **120**, 1788.
- 2 For selected reviews, see: (a) L. C. Miller and R. Sarpong, *Chem. Soc. Rev.*, 2011, **40**, 4550; (b) J. Mahatthananchai, A. M. Dumas and J. W. Bode, *Angew. Chem., Int. Ed.*, 2012, **51**, 10954; (c) G. Zhan, W. Du and Y.-C. Chen, *Chem. Soc. Rev.*, 2017, **46**, 1675; (d) L. Lin and X. Feng, *Chem.–Eur. J.*, 2017, **23**, 6464; (e) Y.-C. Lee, K. Kumar and H. Waldmann, *Angew. Chem., Int. Ed.*, 2018, **57**, 5212; (f) L. Li, Z. Chen, X. Zhang and Y. Jia, *Chem. Rev.*, 2018, **118**, 3752; (g) I. P. Beletskaya, C. Nájera and M. Yus, *Chem. Rev.*, 2018, **118**, 5080; (h) M. Viji, S. Lanka, J. Sim, C. Jung, H. Lee, M. Vishwanath and J.-K. Jung, *Catalysis*, 2021, **11**, 1013.
- 3 For selected examples, see: (a) S. Brandau, E. Maerten and K. A. Jørgensen, *J. Am. Chem. Soc.*, 2006, **128**, 14986; (b) Y. Zhu, X. H. Chen, M. S. Xie, S. X. Dong, Z. Qiao, L. L. Lin, X. H. Liu and X. M. Feng, *Chem.–Eur. J.*, 2010, **16**, 11963; (c) X. Tian, C. Cassani, Y. Liu, A. Moran, A. Urakawa, P. Galzerano, E. Arceo and P. Melchiorre, *J. Am. Chem. Soc.*, 2011, **133**, 17934; (d) H. Shang, Y. Wang, Y. Tian, J. Feng and Y. Tang, *Angew. Chem., Int. Ed.*, 2014, **53**, 5662; (e) J.-Y. Liao, P.-L. Shao and Y. Zhao, *J. Am. Chem. Soc.*, 2015, **137**, 628; (f) W. Du, Q. Gu, Z. Li and D. Yang, *J. Am. Chem. Soc.*, 2015, **137**, 1130; (g) H. V. Adcock, E. Chatzopoulou and P. W. Davies, *Angew. Chem., Int. Ed.*, 2015, **54**, 15525; (h) L. Næsborg, K. S. Halskov, F. Tur, S. M. N. Mønsted and K. A. Jørgensen, *Angew. Chem., Int. Ed.*, 2015, **54**, 10193; (i) T. Hashimoto, H. Nakatsu and K. Maruoka, *Angew. Chem., Int. Ed.*, 2015, **54**, 4617; (j) G. Zhan, M.-L. Shi, Q. He, W.-J. Lin, Q. Ouyang, W. Du and Y.-C. Chen, *Angew. Chem., Int. Ed.*, 2016, **55**, 2147; (k) J.-J. Feng, T.-Y. Lin, C.-Z. Zhu, H. Wang, H.-H. Wu and J. Zhang, *J. Am. Chem. Soc.*, 2016, **138**, 2178; (l) Q.-Q. Cheng, J. Yedoyan, H. Arman and M. P. Doyle, *J. Am. Chem. Soc.*, 2016, **138**, 44; (m) Q.-Q. Cheng, M. Lankelma, D. Wherritt, H. Arman and M. P. Doyle, *J. Am. Chem. Soc.*, 2017, **139**, 9839; (n) L. Wang, S. Li, M. Blgmel, R. Puttreddy, A. Peuronen, K. Rissanen and D. Enders, *Angew. Chem., Int. Ed.*, 2017, **56**, 8516; (o) Y. Deng, L. A. Massey, Y. A. Rodriguez Núñez, H. Arman and M. P. Doyle, *Angew. Chem., Int. Ed.*, 2017, **56**, 12292; (p) D. Uraguchi, R. Shibazaki, N. Tanaka, K. Yamada, K. Yoshioka and T. Ooi, *Angew. Chem., Int. Ed.*, 2018, **57**, 8927; (q) Z. Liu, P. Sivaguru, G. Zanonì, E. A. Anderson and X. Bi, *Angew. Chem., Int. Ed.*, 2018, **57**, 8927; (r) S. Wei, L. Yin, S. R. Wang and Y. Tang, *Org. Lett.*, 2019, **21**, 1458; (s) Y.-H. Wang, J.-S. Tian, P.-W. Tan, Q. Cao, X.-X. Zhang, Z.-Y. Cao, F. Zhou, X. Wang and J. Zhou, *Angew. Chem., Int. Ed.*, 2020, **59**, 1634; (t) H.-K. Liu, S. R. Wang, X.-Y. Song, L.-P. Zhao, L. Wang and Y. Tang, *Angew. Chem., Int. Ed.*, 2019, **58**, 4345; (u) W. Luo, Z. Sun, E. H. N. Fernando, V. N. Nesterov, T. R. Cundari and H. Wang, *Chem. Sci.*, 2020, **11**, 9386; (v) D.-S. Ji, H. Liang, K.-X. Yang, Z.-T. Feng, Y.-C. Luo, G.-Q. Xu, Y. Gu and P.-F. Xu, *Chem. Sci.*, 2022, **13**, 1801; (w) G. Lin, Y. Zhang, H. Zeng, X. Feng, Z. Su and L. Lin, *Chem. Sci.*, 2022, **13**, 4313; (x) Q.-Z. Li, Y.-L. Guan, Q.-W. Huang, T. Qi, P. Xiang, X. Zhang, H.-J. Leng and J.-L. Li, *ACS Catal.*, 2023, **13**, 1164.
- 4 For selected recent reports, see: (a) J. Masson-Makdissi, L. Prieto, X. Abel-Snape and M. Lautens, *Angew. Chem., Int. Ed.*, 2021, **60**, 16932; (b) V. Corti, R. Riccioli, A. Martinelli, S. Sandri, M. Fochi and L. Bernardi, *Chem. Sci.*, 2021, **12**, 10233; (c) C. Portolani, G. Centoze, S. Luciani, A. Pellegrini, P. Righi, A. Mazzanti, A. Ciogli, A. Sorato and G. Bencivenni, *Angew. Chem., Int. Ed.*, 2022, **61**, e202209895; (d) X. Chang, X. Cheng, X.-T. Liu, C. Fu, W.-Y. Wang and C.-J. Wang, *Angew. Chem., Int. Ed.*, 2022, **61**, e202206517; (e) J.-H. Xie, Y.-M. Hou, Z. Feng and S.-L. You, *Angew. Chem., Int. Ed.*, 2023, **62**, e202216396.
- 5 (a) J. Chen, P. Jia and Y. Huang, *Org. Lett.*, 2018, **20**, 6715; (b) B. Cheng, H. Li, X. Zhu, X. Zhang, Y. He, H. Sun, T. Wang and H. Zhai, *Chem. Commun.*, 2021, **57**, 7701.
- 6 (a) I. Nakamura, Y. Sato, K. Takeda and M. Terada, *Chem.–Eur. J.*, 2014, **20**, 10214; (b) B. Riemer, O. Hofer and H. Greger, *Phytochemistry*, 1997, **45**, 337; (c) Y. Shiono, K. Akiyama and H. Hayashi, *Biosci., Biotechnol., Biochem.*, 2000, **64**, 1519; (d) K. M. George, M. Frantz, K. Bravo-Altamirano, C. R. LaValle, M. Tandon, S. Leimgruber, E. R. Sharlow, J. S. Lazo, Q. J. Wang and P. Wipf, *Pharmaceutics*, 2011, **3**, 186; (e) F. Li, J. E. Folk, K. Cheng, M. Kurimura, J. A. Deck, J. R. Deschamps, R. B. Rothman, C. M. Dersch, A. E. Jacobson and K. C. Rice, *Bioorg. Med. Chem.*, 2011, **19**, 4330.
- 7 W. Zheng, W. Yao, N. Ullah and Y. Lu, *Angew. Chem., Int. Ed.*, 2017, **56**, 14222.
- 8 For selected examples, see: (a) Z.-Q. Rong, M. Wang, C. H. E. Chow and Y. Zhao, *Chem.–Eur. J.*, 2016, **22**, 9483; (b) Z.-Q. Rong, L.-C. Yang, S. Liu, Z. Yu, Y.-N. Wang, Z. Y. Tan, R.-Z. Huang, Y. Lan and Y. Zhao, *J. Am. Chem. Soc.*, 2017, **139**, 15304; (c) K.-Q. Chen, Z.-H. Gao and S. Ye, *Org. Chem. Front.*, 2019, **6**, 405; (d) B. M. Trost and Z. Zuo, *Angew. Chem., Int. Ed.*, 2021, **60**, 5806.
- 9 For a review, see: L. Wang, H. Zhu, T. Peng and D. Yang, *Org. Biomol. Chem.*, 2021, **19**, 2110.
- 10 (a) P. Chen, J. Wang, K. Liu and C. Li, *J. Org. Chem.*, 2008, **73**, 339; (b) Q.-M. Li, J.-G. Luo, Y.-M. Zhang, Z.-R. Li, X.-B. Wang, M.-H. Yang, J. Luo, H.-B. Sun, Y.-J. Chen and L.-Y. Kong, *Chem.–Eur. J.*, 2015, **21**, 13206; (c) Q. Luo, X.-Y. Wei, J. Yan, J.-F. Luo, R. Liang, Z.-C. Tu and Y.-X. Cheng, *J. Nat. Prod.*, 2017, **80**, 61.
- 11 (a) X. Liu, K. Wang, Y. Liu and C. Li, *Chem.–Eur. J.*, 2021, **27**, 735; (b) S. Zhang, X. Yu, J. Pan, C. Jiang, H. Zhanga and T. Wang, *Org. Chem. Front.*, 2019, **6**, 3799 For a racemic version, see: (c) K. Verma, I. M. Taily and P. Banerjee, *Org. Biomol. Chem.*, 2019, **17**, 8149.
- 12 (a) H. M. Carder, Y. Wang and A. E. Wendlandt, *J. Am. Chem. Soc.*, 2022, **144**, 11870; (b) C. Che, Y.-N. Lu and C.-J. Wang, *J. Am. Chem. Soc.*, 2023, **145**, 2779.





- 13 For reviews, see: (a) S. J. Connon, *Chem. Commun.*, 2008, 2499; (b) W.-Y. Siau and J. Wang, *Catal. Sci. Technol.*, 2011, **1**, 1298.
- 14 CCDC 2235079 contains the crystallographic data for compound **3f**.
- 15 CCDC 2235267 contains the crystallographic data for compound **4k**.
- 16 (a) T. Gatzenmeier, M. Turberg, D. Yepes, Y. Xie, F. Neese, G. Bistoni and B. List, *J. Am. Chem. Soc.*, 2018, **140**, 12671; (b) G. G. Gerosa, S. A. Schwengers, R. Maji, C. K. De and B. List, *Angew. Chem., Int. Ed.*, 2020, **59**, 20485.
- 17 V. Arun, L. Roy and S. De Sarkar, *Chem.–Eur. J.*, 2020, **26**, 16649.
- 18 I. Harden, F. Neese and G. Bistoni, *Chem. Sci.*, 2022, **13**, 8848.
- 19 B. J. Huffman, T. Chu, Y. Hanaki, J. J. Wong, S. Chen, K. N. Houk and R. A. Shenvi, *Angew. Chem., Int. Ed.*, 2022, **61**, e202114514.
- 20 (a) L. Roy, *Int. J. Quantum Chem.*, 2020, **120**, e26257; (b) M. Baidya and H. Mayr, *Chem. Commun.*, 2008, 1792.
- 21 M. Baidya, D. Maiti, L. Roy and S. De Sarkar, *Angew. Chem., Int. Ed.*, 2022, **61**, e202111679.

